A NOVEL ARRAY PROCESSING METHOD FOR PRECISE DEPTH DETECTION OF ULTRASOUND POINT SCATTER

Konstantinos Diamantis[1], Paul A. Dalgarno[1], Alan H. Greenaway[1], Tom Anderson[2], Jørgen A. Jensen[3] and Vassilis Sboros[1]

[1]School of Engineering & Physical Sciences, Heriot-Watt University, Edinburgh, UK
[2]School of Clinical Sciences, Centre of Cardiovascular Science, University of Edinburgh, UK
[3]Department of Electrical Engineering, Center for Fast Ultrasound Imaging,
Technical University of Denmark, Kgs. Lyngby, Denmark

ABSTRACT

A signal based algorithm resulting in increased depth resolution is presented for medical ultrasound. It relies on multiple foci beamforming that is enabled by current ultrasound imaging systems. The concept stems from optical microscopy and is translated here into ultrasound using the Field II simulation software. A 7 MHz linear transducer is used to scan a single point scatterer phantom that can move in the axial direction. Individual beamformer outputs from 3 different foci are post-processed using the highly-dependent on focusing errors, metric of sharpness to estimate the position of the point scatter. A 37.8 μm uncertainty in depth estimation is achieved, which attains an almost 3-fold improvement compared to conventional ultrasound imaging axial resolution. Future work on the development of this algorithm requires experimental validation in tissue-like materials that provide strong aberrations.

Index Terms— ultrasound imaging, beamforming, multiple focusing, depth-resolution, normalized sharpness

1. INTRODUCTION

A number of sensing fields, such as astronomy and radar, have successfully deployed arrays to resolve point targets with resolution beyond the diffraction limit [1]. On the other hand medical ultrasound has dealt with imaging the structure of human anatomy and has only achieved resolution within the limitations of the beam diffraction. Higher resolution, here, is achieved by increasing frequency at the expense of sacrificing penetration depth [2, 3]. However, super-resolution methods in fields such as optical microscopy [4] should be possible to translate into ultrasound imaging as the basic physics principles are similar. Indeed, new work shows that the localization of microbubble scatter [5] resulted in high resolution images of vascular structure [6, 7].

Optical methods [8] based on the understanding of the Point Spread Function (PSF) have managed to achieve down to $\lambda/10$ lateral resolution. Past work [9] has used the image sharpness metric to extend the resolution gains to the depth dimension. Image sharpness is defined as the integrated square intensity over the emitter, and was mainly used in astronomy for correction of distorted images [10]. This measure has been adopted in biological microscopy for the high precision depth detection of fluorescent particles [11, 12]. The method combines multiplane microscopy [13], a maximum likelihood algorithm, and sharpness to provide an average of approximately 14 nm depth resolution when applied to images of unresolved targets (λ=532 nm). In this work, the technique is introduced in ultrasonics, where the multiplane imaging has been replaced by signal processing, and is validated with Field II [14, 15] simulated ultrasound data.

This work is supported by Heriot-Watt University, and by grant 82-2012-4 from the Danish Advanced Technology Foundation.

2. METHODS

2.1. Sensor Signal Processing

Transmission of ultrasound is performed through focused beams. From each transmission one line is formed by beamforming the received sensor signals, and combining lines from multiple transmissions will then form the image. The standard way to process the received responses is the Delay-And-Sum (DAS) beamformer [16]. The signals are time-delayed, weighted, and finally summed to form the maximized output, $B(t)$, that for M emissions is given by:

$$B(t) = \sum_{m=0}^{M-1} w_m(t) x_m(t - \tau_m) = \mathbf{w}(t)^H X(t)\,, \quad (1)$$

where t is the time, $\mathbf{w}(t) = [w_0(t), w_1(t), ..., w_{M-1}(t)]^H$ is the vector of the elements weighting (apodization), $X(t) = [x_0(t-\tau_0), x_1(t-\tau_1), ..., x_{M-1}(t-\tau_{M-1})]^H$ is the array of the sensor signals, and τ_m is the time delay applied to the mth element, calculated by its distance from the focal depth. Eq. (1) can be applied individually for more than one τ_M, thus fixed receive focus. This will result in different beamformer outputs and different images of the same object.

Here the object is a point scatterer that changes depth position between acquisitions, and for each position the algorithm uses similar processing as described in [11, 12]. Hence, three foci are employed in receive and three sharpness values are calculated for a particular depth. The sharpness metric in optics is usually extracted by pixel intensities of an image and there is no unique way to assess its value [17]. It is a measure of image quality, dominated by defocus. It becomes maximum for in-focus images and declines rapidly and symmetrically as defocus increases [10]. A normalized version of sharpness has been adopted for ultrasound data and is defined by:

$$S = \sum_{q=1}^{Q} A_q^4 / (\sum_{q=1}^{Q} A_q^2)^2 \,, \tag{2}$$

where S is the normalized sharpness, Q is the number of samples including one point target, and A_q is the amplitude value of the q^{th} sample. For the calculation, the signals from the beamformer outputs [18] have been preferred instead of images [11], to avoid further processing involved until the image formation stage is reached. The pixel intensity is generally proportional to the square of the signal amplitudes, thus the 4^{th} order term in eq. (2). In the presence of multiple scatterers in an image, the sharpness calculation remains unaffected on condition that the number of samples Q is reduced to always enclosing a single PSF.

2.2. Statistical Post-processing

Consecutive sharpness values plotted over scatterrer position will form a sharpness curve (S-curve). For each of the three foci used in receive, a separate S-curve can be created, which results in three curves. The algorithm aims to estimate a unique point scatterer position based on its triple characterization by three distinct sharpness values. The accuracy of the method is determined by repeating the whole process several times with the objective to estimate a probability density function (PDF), $P(S_j|z)$. This is the probability of the normalized sharpness value, S_j, calculated from the beamformed data of a point scatterer located at depth z, where j denotes the specific receive focus. The sharpness calculations for each receive focus, are independent from each other and with z known, the probability for N sharpness measurements for all receive foci when a point scatterer is located at z can be written as:

$$L(S_1, S_2, ..., S_N|z) = \prod_{j=1}^{N} P(S_j|z) \,, \tag{3}$$

where L is the likelihood for the total sharpness measurements $S_1, S_2, ..., S_N$ and N is the number of the different selected receive foci. The maximum likelihood estimator (MLE) of the particle depth, z, is the value of z for which L is maximized providing as input an actual measured dataset $S_1, S_2, ..., S_N$ and the calibration PDFs, $P(S_j|z)$. The mean and the standard deviation of the measured sharpness data are extracted and a Lorentzian fit is applied to both the mean S-curve and its associated deviation [11]. The fitted data are then interpolated to construct more data points that will increase the method's accuracy. For the PDF a Gamma distribution has been chosen as it fits best the shape of the S-curves and is given by:

$$P(S_j|z) = \frac{e^{\bar{S}_j^2} \bar{S}_j^{\alpha-1}(z) \beta^{-\alpha}}{\Gamma(\alpha)} \,, \tag{4}$$

where $\alpha = \bar{S}_j^2(z)/\bar{\sigma}_j^2$ and $\beta = \bar{\sigma}_j^2/\bar{S}_j^2(z)$. $\bar{S}_j(z)$ denotes the interpolated Lorentzian fit of the mean S-curve, $\bar{\sigma}_j^2$ the interpolated Lorentzian fit of the sharpness variance, both extracted by multiple simulations, and Γ is the Gamma function. The estimated depth position is finally compared with the true depth defined by the simulation setup. The whole algorithm steps are depicted in Algorithm 1.

Algorithm 1 Multiple focusing for precise depth detection

for $z = z_{start}$ to z_{end} **do**
  Create phantom including a point target at depth z
  for $i = 1$ to NumFrames **do**
    Emit 128 focused waves from the active aperture
    Collect and store raw RF data from all emissions
    for $j = 1$ to N **do**
      Beamform acquired data according to eq. (1)
      with fixed focus j in receive
    end for
  end for
end for
Calculate all sharpness values $S_{z,i,j}$ based on eq. (2)
Calculate statistical measures from sharpness data
  -Extract mean sharpness values for each position
  -Extract the standard deviation from mean values
Plot mean S-curves and associated deviation over depth
Apply Lorentzian fits to mean S-curves & deviation
Interpolate the fitted data by a K factor
Select the PDF model and insert interpolated data
Receive depth estimates and compare with actual depth

2.3. Simulation Setup

A linear 7 MHz, 192 element, simulated transducer with λ spacing was used to scan a phantom, which includes a single point target at an initial depth of 32.5 mm and below the central transducer element. The transmitting aperture consists of 64 elements, and the scanning is performed by translating the 64 active elements over the aperture and focus at the selected depth. In this study, two individual cases have been explored, one with the transmit focus set to 30 mm and the other where the focal depth is at 50 mm. The speed of sound, c is set to

1540 m/s and the wavelngth is $\lambda = c/f_0 = 220$ μm. All simulations have been carried out with the Field II [14, 15] software and Matlab scripts have been written for the data post-processing.

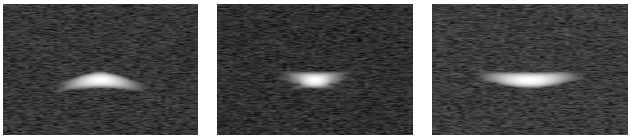

(a) r_{foc}=38 mm (b) r_{foc}=40 mm (c) r_{foc}=42 mm

Fig. 1. Random example of three PSFs of the same RF dataset that has been beamformed with three different foci in receive. White Gaussian noise with an SNR=10 dB has been added to the signals. The transmit focus is set to 30 mm and the actual location of the target is $(x, z) = (0, 39.5)$ mm. From each PSF a sharpness value is assessed. Images are displayed with a 60 dB dynamic range.

Raw data from 128 focused emissions are acquired and stored before a new phantom is created, with the point scatterer moved 100 μm (z-step) away from the transducer face until the end depth of 47.5 mm. As a result, 151 acquisitions are done in total with the scatterer covering a distance of 15 mm. Data from each acquisition are beamformed with three receive foci placed at 38, 40 and 42 mm respectively. Fig. 1 shows a random example of three beamformed responses for the three selected foci in receive (r_{foc}).

3. RESULTS

By following the steps of Algorithm 1 and by using the current scan parameters, for each of the three receive foci, 151 normalized sharpness values are calculated leading to the generation of three S-curves. Ten sharpness datasets are created where 10 dB white Gaussian noise has been added to the raw signals. This allows the extraction of the mean S-curves and their variance that are necessary for the MLE analysis. The Lorentzian fits applied to the sharpness data are interpolated by a factor $K = 1000$, using the Matlab spline interpolation function and are embedded in the Gamma PDF model. The depth vector following the sharpness data interpolation is also updated and the new z-step becomes $0.1/1000$ mm. A set of three measured sharpness values are the PDF's input and the output is the depth estimate for which the PDF becomes maximum with an estimation error equal to the modulated step. This estimate is compared with the already known, from the simulation setup, position and the same is repeated for all 151 datasets.

Simulations with the transmit focus set to 30 mm and to 50 mm are two separate studies. In Fig. 2a the three mean S-curves are displayed for the first case, and the absolute difference between estimated and actual depths can be found in Fig. 2b. The sharpness values shown at 39.5 mm have been

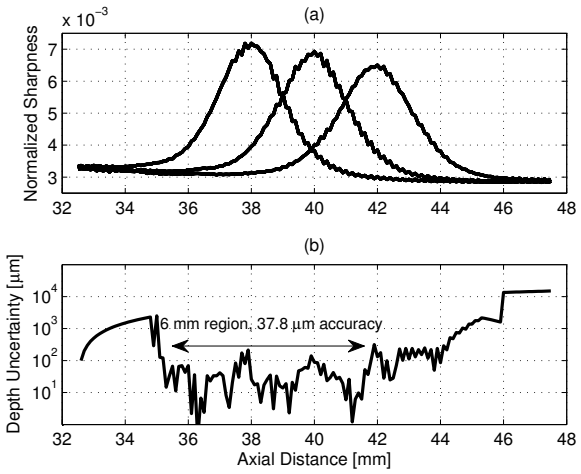

Fig. 2. (a) A set of three normalized S-curves from a simulated ultrasound point target moving in depth. Data have been generated by focused at 30 mm ultrasound transmission and by beamforming with three different foci in receive. Three sharpness values for each particle position result in depth estimation with accuracy of 37.8 μm between 35.5 and 41.5 mm as shown in (b).

extracted by the PSFs shown in Fig. 1. There is an approximately 6 mm region (from 35.5 mm to 41.5 mm) where the localization error is on average, 37.8 μm or 0.17λ (arrowed region in Fig. 2b). In Fig. 3a the equivalent curves are shown for the case of the 50 mm transmit focus. As previously, there is again a 6 mm region where the localization error is on average 34.3 μm or 0.15λ. This value is slightly lower than before, and thus the highest resolution obtained. It demonstrates a 3.2-fold improvement compared to the conventional axial resolution that is approximately around $\lambda/2 = 110$ μm [3]. However this time, the super-resolution area is located between 38.5 mm to 44.5 mm as indicated by the arrow in Fig. 3b.

4. DISCUSSION

A technique that can achieve axial resolution down to $\lambda/6$ in point scatterer detection is proposed. The method is translated from localisation microscopy, where it has reached $\approx \lambda/40$ depth resolution, into ultrasound. Here common ultrasound imaging sequences with one transmit focus and 3 receive foci were implemented, similar to those clinically used. This result merits further research to develop the algorithm and investigate the potential for futher resolution gains. Parameters like the way of ultrasound transmission, the acquisition time, the depth of interest, the velocity of the moving scatterer or the S-curvve fit need to be examined to define perspectives and limitations. Experimental validation with real point scatterers will be required to demonstrate the usefulness of the

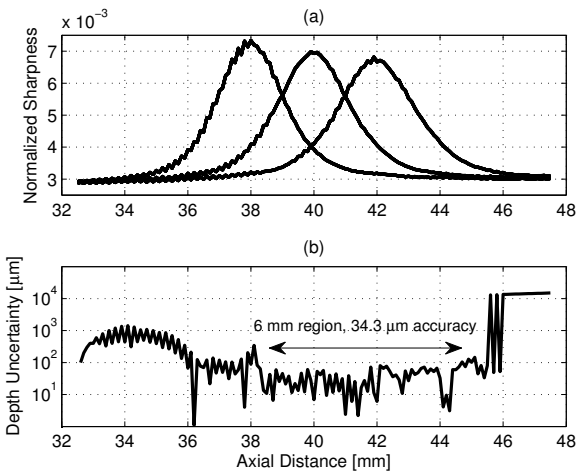

Fig. 3. (a) Three S-curves as in Fig. 2 but with the transmit focus set to 50 mm. (b) Depth estimation with maximum accuracy of 34.3 μm between 38.5 and 44.5 mm is achieved based on the sharpness method.

method. The sharpness technique may add to the new super-resolution image based methods for the detection of contrast microbubbles [6, 7], as it is signal based and may help reduce significantly the PSF variability, prior to image analysis, which is an important limitation of ultrasound imaging.

The results (Figs. 2a and 3a) show that the positions of both transmit and receive focus have a significant effect on the S-curves. Each curve peak is located at the receive focus point as expected, with shorter receive foci resulting in higher curve peaks due the smallest distance between r_{foc} and transducer face. However, the curve symmetry that is present in the optical example is distorted due to the introduction of the transmit focus. When the transmit focus is set to the left of the curves (30 mm) the left halves of all curves are slightly shifted to higher sharpness values and increased variability is noticed in the right halves away from transmit focus (Fig. 2a). Exactly the opposite can be observed in Fig. 3a where the focus is set after the furthest position of the scatterer (50 mm). In this case the right half of each curve appears slightly shifted to higher values and in the left halves that are furthest away from the focus flickering is introduced. This variation in Figs. 2a and 3a is best reflected in Figs. 2b and 3b. There is a common 3 mm super-resolution depth range (from 38.5 to 41.5 mm) but a further 3 mm range is located once on the left and once on the right of the central area for the respective transmit foci. In both cases the uncertainty becomes much higher for depth estimates outside the 6 mm range. This is because there is no signigicant change between neighboring sharpness values at this part of the curves which is essential for this technique. Despite this shift in the high resolution area, the resolution gains are very similar for both transmit foci.

It is important to mention that, in practice, whereas the transmit focus can only be chosen once for each acquisition, multiple receive foci can be used since the acquired data can be beamformed with different time-delays. As a consequence the number of S-curves that can be formed is practically unlimited, in contrast to multiplane microscopy where hardware limitations are imposed [11], and this may increase the range of the high-precision depth detection to cover the entire image. As the resolution gains are not affected it is shown that strong ultrasound field aberration, which includes defocus, does not affect the performance of the technique in achieving super-resolution localisation. Importantly the shift in the high resolution area indicates a potentially significant advantage of the sharpness method over other adaptive techniques, such as minimum variance [19]. Tissue and the complex structure of the human body increase ultrasound aberrations at the position of focus. Future experimental work will demonstrate whether the sharpness method is affected by real imaging aberrations. As stated above, in the case that there is only a shift in the high resolution area this can be dealt with multiple receive foci placed adaptively to ensure uniform resolution performance across the image.

5. CONCLUSION

Multiple normalized sharpness values can be assessed through offline beamforming, for a simulated ultrasound point scatterer that moves in depth. The sharpness data plotted over scatterer displacement will form curves whose symmetry and peak depend on the position of the transmit and receive focus respectively. Despite the increased fluctuations, the general shape of these ultrasound curves is similar to those obtained in biological microscopy where sharpness has been used for particle tracking. Based on this, the algorithm can be reproduced for ultrasound data only by substituting the image analysis part with signal processing. The precision in depth detection reaches 34.3 μm (0.15λ) for a 6 mm range depending on the transmit parameters of the scan. The presented technique shows promising results, but detailed analysis of the sharpness behavior is required, before it can be applied to real-time data.

6. REFERENCES

[1] S. Haykin, J. H. Justice, N. L. Owsley, J. L. Yen, and A. C. Kak, "Array Signal Processing," Englewood Cliffs, NJ: Prentice Hall, 1985.

[2] P. Hoskins, K. Martin, and A. Thrush, "Diagnostic Ultrasound: Physics and Equipment," (2nd. ed.) Cambridge University Press, 2010.

[3] M. L. Oelze, and W. D. O'Brien, Jr., "Defining optimal axial and lateral resolution for estimating scatterer properties from volumes using ultrasound backscatter,"

J. Acoust. Soc. Am., vol. 115, no. 6, pp. 3226-3234, 2004.

[4] E. Betzig, G. H. Patterson, R. Sougrat, O. W. Lindwasser, S. Olenych, J. S. Bonifacino, M. W. Davidson, J. Lippincott-Schwartz, and H. F. Hess, "Imaging intracellular fluorescent proteins at nanometer resolution," *Science*, vol. 313, no. 5793, pp. 1642-1645, 2006.

[5] V. Sboros, C. M. Moran, S. D. Pye, and W. N. McDicken, "The behaviour of individual contrast agent microbubbles," *Ultr. Med. Biol.*, vol. 29, no. 5, pp. 687-694, 2003.

[6] M. A. O'Reilly, R. M. Jones, and K. Hynynen, "Three-dimensional transcranial ultrasound imaging of microbubble clouds using a sparse hemispherical array," *IEEE Trans. Biom. Eng.*, vol. 61, no. 4, pp. 1285-1294, 2014.

[7] K. Christensen-Jeffries, R. J. Browning, M. X. Tang, C. Dunsby, and R. J. Eckersley, "*In Vivo* Acoustic Super-Resolution and Super-Resolved Velocity Mapping Using Microbubbles," *IEEE Trans. Med. Imag.*, vol. 34, no. 2, pp. 433-440, February 2015.

[8] A. L. McEvoy, D. Greenfield, M. Bates, J. Liphardt, "Q&A: Single-molecule localization microscopy for biological imaging," *BMC Biology*, vol. 8, no. 106, 2010.

[9] Y. Sun, J. D. McKenna, J. M. Murray, E. M. Ostap, and Y. E. Goldman, "Parallax: high accuracy three-dimensional single molecule tracking using split images," *Nano Lett.*, vol. 9, no. 7, pp. 2676-2682, 2009.

[10] R. A. Muller, and A. Buffington, "Real-time correction of atmospherically degraded telescope images through image sharpnening," *J. Opt. Soc. Am*, vol. 64, no. 9, pp. 1200-1210, September 1974.

[11] H. I. C. Dalgarno, P. A. Dalgarno, A. C. Dada, C. E. Towers, G. J. Gibson, R. M. Parton, I. Davis, R. J. Warburton, and A. H. Greenaway, "Nanometric depth resolution from multi-focal images in microscopy," *J. R. Soc. Interface*, vol. 8, no. 60, pp. 942-951, July 2011.

[12] P. A. Dalgarno, H. I. C. Dalgarno, A. Putoud, R. Lambert, L. Paterson, D. C. Logan, D. P. Towers, R. J. Warbuton, and A. H. Greenaway, "Multiplane imaging and three dimensional nanoscale particle tracking in biological microscopy," *Opt. Expr.*, vol. 18, no. 2, pp. 877-884, 2010.

[13] P. M. Blanchard, and A. H. Greenaway, "Simultaneous multiplane imaging with a distorted diffraction grating," *Appl. Opt.*, vol. 38, no. 32, pp. 6692-6699, 1999.

[14] J. A. Jensen, "Field: A Program for Simulating Ultrasound Systems," *Med. Biol. Eng. Comp.*, vol. 10th Nordic-Baltic Conference on Biomedical Imaging, Vol. 4, Supplement 1, Part 1, pp. 351-353, 1996.

[15] J. A. Jensen and N. B. Svendsen, "Calculation of pressure fields from arbitrarily shaped, apodized, and excited ultrasound transducers," *IEEE Trans. Ultrason., Ferroelec., Freq. Contr.*, vol. 39, pp. 262-267, 1992.

[16] K. E. Thomenius, "Evolution of ultrasound beamformers," *Proc. IEEE Ultrason. Symp.*, pp. 1615-1622, 1996.

[17] N. K. Chern, P. A. Neow, M. H. Ang Jr., "Practical issues in pixel-based auto focusing for machine vision," *Proc. IEEE Robotics and Automation*, pp. 2791-2796, May 2001.

[18] I. M. Rosado-Mendez, T. J. Hall, and J. A. Zagzebski, "Pulse-echo sound speed estimation based on a Nakagami model of the echo amplitude," *Proc. IEEE Ultrason. Symp.,* pp. 2442-2445, Sep. 2014.

[19] K. Diamantis, I. H. Voxen, A. H. Greenaway, T. Anderson, J. A. Jensen, and V. Sboros, "A comparison between temporal and subband minimum variance adaptive beamforming," *in Proc. SPIE Med. Imag.*, vol. 9040, March 2014, 90400L. [Online]. Available: 10.1117/12.2043602